INTERIM PROGRESS REPORT

JPL P. O. No. AX5-368523

MECHANICAL VIBRATION TRANSMISSION IN THE MARINER '69 SPACECRAFT

14 July 1967

GPO PRICE $ _____

CFSTI PRICE(S) $ _____

Hard copy (HC) 3.00

Microfiche (MF) .65

ff 653 July 65

Submitted to:

California Institute of Technology
Jet Propulsion Laboratory
4800 Oak Grove Drive
Pasadena, California 91103

Attention: Marc C. Trummel
Mail Station 126-240

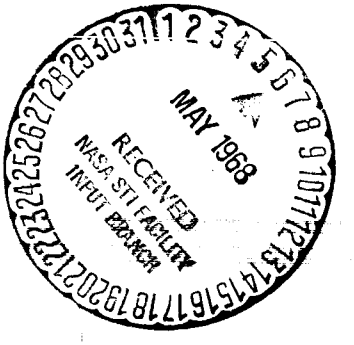

INTERIM PROGRESS REPORT

JPL P. O. No. AX5-368523

MECHANICAL VIBRATION TRANSMISSION IN THE MARINER ' 69 SPACECRAFT

14 July 1967

Submitted to:

California Institute of Technology
Jet Propulsion Laboratory
4800 Oak Grove Drive
Pasadena, California 91103

Attention: Marc C. Trummel
Mail Station 126-240

This work was performed for the Jet Propulsion Laboratory, California Institute of Technology, sponsored by the National Aeronautics and Space Administration under Contract NAS7-100.

TABLE OF CONTENTS

MECHANICAL VIBRATION TRANSMISSION IN THE MARINER '69 SPACECRAFT

I. INTRODUCTION

This report describes an analytical procedure for estimating vibration transmission in the Mariner '69 spacecraft assembly. The mechanical vibration transmission path considered involves the following elements: (1) the Centaur tank-dome or alternatively the vibration test fixture, (2) the adapter stiffeners, (3) the ring frame, and (4) the spacecraft electronic-assembly panels (Fig. 1). Analytical predictions of the acceleration transfer functions for these elements are compared with octave-band measurements of the transfer functions. Acoustical vibration transmission paths will be considered in a follow-on study, and the relative importance of the various transmission paths will be assessed.

The analytical predictions are based on "statistical energy analysis" techniques which have been previously described[1] and utilized to predict vibration transmission in a model of the OGO spacecraft.[2] These techniques are ideally suited to the calculation of high frequency sound and vibration transmission, because application of the techniques does not require knowledge of the acoustic and vibration mode shapes and the resonance frequencies which depend on the fine details of spacecraft elements and their interconnections. However, these techniques are only applicable when several vibration modes occur in the analysis frequency band; so the techniques are not suited to low-frequency or narrow-band analyses of vibration transmission.

Statistical energy analysis techniques yield predictions of the mean-square vibration response averaged over a frequency band and over a uniform spatial region. Fortunately, at

MECHANICAL VIBRATION TRANSMISSION IN THE MARINER '69 SPACECRAFT

I. INTRODUCTION

This report describes an analytical procedure for estimating vibration transmission in the Mariner '69 spacecraft assembly. The mechanical vibration transmission path considered involves the following elements: (1) the Centaur tank-dome or alternatively the vibration test fixture, (2) the adapter stiffeners, (3) the ring frame, and (4) the spacecraft electronic-assembly panels (Fig. 1). Analytical predictions of the acceleration transfer functions for these elements are compared with octave-band measurements of the transfer functions. Acoustical vibration transmission paths will be considered in a follow-on study, and the relative importance of the various transmission paths will be assessed.

The analytical predictions are based on "statistical energy analysis" techniques which have been previously described[1] and utilized to predict vibration transmission in a model of the OGO spacecraft.[2] These techniques are ideally suited to the calculation of high frequency sound and vibration transmission, because application of the techniques does not require knowledge of the acoustic and vibration mode shapes and the resonance frequencies which depend on the fine details of spacecraft elements and their interconnections. However, these techniques are only applicable when several vibration modes occur in the analysis frequency band; so the techniques are not suited to low-frequency or narrow-band analyses of vibration transmission.

Statistical energy analysis techniques yield predictions of the mean-square vibration response averaged over a frequency band and over a uniform spatial region. Fortunately, at

high frequencies, the frequency and spatial variations in response of multimodal aerospace-type structures are generally quite small. In this report, the space-average, mean-square acceleration responses of the spacecraft assembly elements are calculated as a function of frequency. These response calculations are comparable to data obtained by averaging acceleration spectra measured at a number of positions on a structural element and then smoothing the average spectrum in frequency.

The vibration transmission model of the Mariner '69 spacecraft assembly is shown in Fig. 1. The model is, of course, quite idealized and does not contain all the complexities of the actual spacecraft construction. The electronic module boards in the Mariner bus are attached to eight panels which are connected in the form of an octagon. The primary goal of this study is to calculate the vibration transmitted from the spacecraft adapter into these panels. The vibration transmission model consists of the eight spacecraft panels (4), attached at eight feet to a stiff ring frame (3) at the upper end of the adapter (Fig. 1). The adapter is modeled as a cylindrical shell with axial stiffeners (2). To model the flight configuration, we assume that the adapter is mounted on a spherical section of tank dome (1a); and to model the laboratory vibration configuration, we assume the adapter is mounted on a rigid test fixture (1b).

In our calculations, the structural elements of the model are completely characterized by gross properties such as: mass, modal density, and input point impedances calculated for infinite and semi-infinite structures. To simplify the calculations, we have neglected the stiffening effects of

the ring frame and tank dome curvature on their modal densities and input point impedances. The effects of curvature are not important above the ring frequency:

$$f_r = \frac{C_\ell}{2\pi a}$$

where C_ℓ is the speed of longitudinal waves in the bulk material and a is the radius of curvature. (For the ring frame and tank dome with C_ℓ = 17,000 ft/sec and a = 2.5 ft, $f_r \approx$ 1000 Hz.) Below the ring frequency, our calculations are approximate and should be refined at a later date.

In Section II of this report, power balance equations relating the response of adjacent elements of the spacecraft model are formulated; in Section III, modal densities are discussed; in Section IV, the coupling loss factors are calculated; and in Section V, the acceleration response ratios for the structural elements are presented. The results of an analytical and experimental study of vibration transmission between two plates is presented in the appendix.

II. POWER BALANCE FORMULATION

In this section we formulate power balance equations governing the vibration responses of the elements of the model shown in Fig. 1. These structure-to-structure power balance equations are based on results for the power flow between the vibration modes of each structural element. Because of the structural constraints of the model shown in Fig. 1, only the following types of vibration modes of each element are considered.

(1a) Tank Dome -- bending vibration modes
(1b) Test Fixture -- horizontal translation (one mode)
(2) Adapter Stiffeners -- bending vibration modes with motion perpendicular to the adapter shell
(3) Ring Frame -- bending vibration modes with motion perpendicular to the adapter shell
(4) Spacecraft Panels -- bending vibration modes

In formulating the power balance equations for the model, we will study four structural elements in sets of two--thus, we will first study the ring frame and spacecraft panels, then the adapter stiffeners and ring frame, etc. To be completely correct, one should study the four elements as a system in writing the power balance equations. However, the former simple approach may be shown to be valid in both the limiting cases where: (1) the coupling loss factors are very small compared to the internal loss factors, or (2) the coupling loss factors are very large compared to the internal loss factors.

A. Ring Frame and Spacecraft Panels

According to statistical energy analysis,[1] the time-average power flow from the ring frame to the spacecraft panels is proportional to the difference in the time average modal energies of the ring frame and spacecraft and is given by:

$$\langle P_{rs} \rangle = \omega_o \, \eta_{rs} \, N_r \left[\frac{\langle E_r \rangle}{N_r} - \frac{\langle E_s \rangle}{N_s} \right] \qquad (1)$$

where ω_o is the central radian frequency of a frequency band $\Delta\omega$, η_{rs} is the coupling loss factor from the ring frame to the spacecraft panels, N is the total number of vibration modes in a frequency band, and <E> is the time average total energy. (The subscript, r, denotes the ring frame and s the spacecraft panels and <...> denotes a time average.)

The time-average power dissipated internally in the spacecraft panels is:

$$\langle P_s^{diss} \rangle = \omega_o \, \eta_s \, \langle E_s \rangle \qquad (2)$$

where η_s is the internal loss factor of the spacecraft panels.

Assuming that all the time average power transmitted from the ring frame to the spacecraft panels is dissipated internally in the spacecraft panels, we equate Eqs. 1 and 2 to obtain:

$$\frac{\langle E_s \rangle}{\langle E_r \rangle} = \frac{\eta_{rs}}{\eta_s + \frac{N_r}{N_s}\eta_{rs}} \quad . \qquad (3)$$

Since the total energy is related to the space-average mean square acceleration $\langle A^2 \rangle_{s,t}$ of a structure by:

$$E = \frac{M}{\omega_o^2} \langle A^2 \rangle_{s,t} \quad , \qquad (4)$$

where M denotes the structure mass and $\langle \ldots \rangle_{s,t}$ denotes the space-time average and since the coupling loss factors and number of modes are related by the reciprocity relation:[1/]

$$N_s \eta_{sr} = N_r \eta_{rs} \quad , \qquad (5)$$

we can rewrite Eq. 3 as:

$$\frac{\langle A_s^2 \rangle_{s,t}}{\langle A_r^2 \rangle_{s,t}} = \frac{M_r}{M_s} \frac{N_s}{N_r} \frac{\eta_{sr}}{\eta_{sr}+\eta_s} \quad . \qquad (6)$$

B. Adapter Stiffeners and Ring Frame

Since the adapter stiffeners and the ring frame are both intimately connected to the adapter shell, we assume that the time average modal energies of the adapter stiffeners and the ring frame are equal:

$$\frac{\langle E_a \rangle}{N_a} = \frac{\langle E_r \rangle}{N_r} \quad ,$$

where the subscript, a, denotes the adapter stiffeners.

Using Eq. 4, the ratio of the ring frame acceleration to the adapter stiffener acceleration is:

$$\frac{\langle A_r^2 \rangle_{s,t}}{\langle A_a^2 \rangle_{s,t}} = \frac{M_a \, N_r}{M_r \, N_a} \tag{7}$$

(Notice that we could alternately have derived Eq. 7 by considering the power flow from the adapter stiffeners to the ring frame, deriving an equation analogous to Eq. 6, and assuming that $\eta_{ra} >> \eta_r$ which follows from the fact that the ring frame is tightly coupled to the adapter stiffeners.)

C. Tank Dome and Adapter Stiffeners

The ratio of the adapter stiffener acceleration to the tank dome acceleration is calculated by considering the power flow from the tank dome to the adapter stiffeners. The steps involved are identical with those in Section A, and we write down the result by replacing the subscripts s and r of Eq. 6 with a and t respectively:

$$\frac{\langle A_a^2 \rangle_{s,t}}{\langle A_t^2 \rangle_{s,t}} = \frac{M_t \, N_a}{M_a \, N_t} \frac{\eta_{at}}{\eta_{at}+\eta_a} \quad , \tag{8}$$

where the subscript t refers to the tank dome.

D. Test Fixture and Adapter Stiffeners

Similarly, the ratio of the adapter stiffener acceleration to the test fixture acceleration is written by replacing the subscripts s and r of Eq. 6 with a and f respectively:

$$\frac{\langle A_a^2 \rangle_{s,t}}{\langle A_f^2 \rangle_{s,t}} = \frac{M_f N_a}{M_a} \frac{\eta_{af}}{\eta_{af}+\eta_a} \quad , \tag{9}$$

where the subscript f refers to the test fixture and we have taken the number of fixture modes as one.

The response ratios given by Eqs. 6-9 depend on the spacecraft structural element masses, number of modes, coupling loss factors, and internal loss factors. When the coupling loss factors η_{ij} that appear in these expressions are large compared to the internal loss factors η_i, the response ratios are independent of the coupling and internal loss factors and depend only on the masses and modal densities (see Eq. 7). Unfortunately, we would expect the coupling loss factors from the spacecraft to the ring frame and from the adapter stiffeners to the fixture to be smaller than the internal loss factors of the spacecraft panels and the adapter stiffeners respectively. For example, if we excited the spacecraft panels directly with a number of small shakers, we would expect the energy to be dissipated internally in the panels and electronic assemblies faster than the energy

would leak out through the feet into the ring frame. We might expect the coupling loss factor from the adapter stiffeners to tank dome to be of the same order of magnitude as the internal loss factor of the adapter stiffeners.

The masses of the spacecraft elements are estimated from design drawings of the spacecraft assemblies. The number of modes are calculated from the modal densities which depend only on the overall dimension and physical properties of the elements as described in Section III. The coupling loss factors can be measured or calculated from infinite system models as we demonstrate in Section IV. The internal loss factors, which characterize the internal damping of the elements, must be measured or estimated from past experience.

III. MODAL DENSITIES

The response ratios in Eqs. 6-9 depend on N_i, the number of vibration modes of the $i^{\underline{th}}$ element with resonance frequencies in the analysis frequency band, $\Delta\omega$. To estimate the number of modes in a frequency band, $\Delta\omega$, it is convenient to introduce the concept of a "modal density", n_i, defined as the number of modes of the $i^{\underline{th}}$ element in a unit frequency band:

$$n_i \equiv \left.\frac{N_i}{\Delta\omega}\right|_{\Delta\omega \to o} \tag{10}$$

The number of modes in the frequency band, $\Delta\omega$, is of course then given by:

$$N_i = n_i \Delta\omega \tag{11}$$

From Eq. 11, it is evident that the modal density concept is valid only in the frequency range where several modal resonance frequencies fall within the analysis frequency bandwidth.

The usefulness of the modal density concept stems primarily from the fact that--at frequencies above the first few resonance frequencies of a structure where the vibration wavelengths are small compared with the structural dimensions--the modal density of a structure is independent of the boundary conditions and depends only on the gross geometric and physical properties of the structure. The modal densities of a number of simple structural and acoustical

elements have been calculated and tabulated.[3] The modal density of complex built-up structures can be estimated by adding the modal densities of the constituent elements. For example, the modal density of a ribbed panel equals the modal density of the ribs plus the modal density of the panel.

To illustrate the calculation of modal densities, consider a simple pinned-pinned steel beam 1/16 in. thick and 3 ft in length. The resonance frequencies of the beam are derived from the characteristic equation:

$$\omega_m = \frac{m^2\pi^2}{L^2} C_\ell \kappa \tag{12}$$

where m is the mode number, C_ℓ is the longitudinal speed of sound (~17,000 ft/sec in steel and aluminum), κ is the radius of gyration ($1/2\sqrt{3}$ times the thickness for a beam of uniform cross-section), and L is the beam length. The number of modes $N(\omega)$ with resonance frequencies below ω is obtained by solving Eq. 12 for m:

$$N(\omega) = m = \frac{L}{\pi}\sqrt{\frac{\omega}{C_\ell \kappa}}$$

and the beam modal density is given by:

$$n_b(\omega) = \frac{d\,N(\omega)}{d\omega} = \frac{L}{2\pi}\frac{1}{\sqrt{\omega C_\ell \kappa}} \tag{13}$$

Thus, the modal density of the beam in our example is:

$$n(\omega) \simeq 1/10\sqrt{\omega}$$

and we would expect 7 modes between 1000 and 2000 Hz. (NOTE: the modal densities defined in terms of cyclic frequency and radian frequency are related by $n(f) = 2\pi\, n(\omega)$).

To calculate the number of modes of the ring frame and the adapter stiffeners in a frequency band, $\Delta\omega$, we use Eqs. 11 and 13. To calculate the number of modes of the spacecraft panels and the tank dome, we use Eq. 11 and the expression for the modal density of a flat plate:[3]

$$n_p(\omega) = \frac{\sqrt{3A}}{2\pi\, C_\ell h} \quad , \qquad (14)$$

where A is the area of the plate. Below the ring frequency (approximately 1000 Hz), the ring frame and tank dome have a few less modes than Eqs. 13 and 14 predict.

IV. COUPLING LOSS FACTORS

Since the coupling loss factors between an element, i, and an element, j, are related by the reciprocity relation:[1]

$$n_i \eta_{ij} = n_j \eta_{ji} \tag{15}$$

we can calculated either η_{ij} or η_{ji} and obtain the reciprocal coupling loss factor from Eq. 15 and the modal densities.

A. Ring Frame to Spacecraft Panel Coupling Loss Factor

Two types of motion at the spacecraft-panel, ring-frame junction result in power transmission into the spacecraft panels: (1) torsional motion about the line joining adjacent spacecraft panels, and (2) radial motion perpendicular to the ring frame and the spacecraft panels. The radial motion is somewhat inhibited by the stiff octagonal construction of the spacecraft-panel assembly but an experimental investigation of vibration transmission between two panels (see the appendix) demonstrated that even small radial motion can result in large power transmission. In this section, we give a detailed calculation of the coupling loss factor due to torsional motion and give only the final result for radial motion.

To calculate the ring frame to spacecraft coupling loss factor, η_{rs}, for torsional motion along the spacecraft panel junctions, we consider Eq. 1 for the case where the energy of the spacecraft panels is essentially zero:

$$\eta_{rs} = \frac{\langle P_{rs} \rangle}{\omega_o \langle E_r \rangle} \Bigg| \langle E_s \rangle = 0 \qquad (16)$$

We apply Eq. 16 to the semi-infinite spacecraft-panel and ring frame model shown in Fig. 2 and calculate the coupling loss factor.

First, we calculate the power transmitted through one ring-frame, spacecraft-panel junction when a bending wave of unit amplitude traveling along the ring frame impinges on the junction. Assume an incident wave with motion perpendicular to the ring frame and the spacecraft panels traveling to the right along the ring frame:

$$w = e^{i\ (k_r x - \omega t)}$$

where k_r is the bending wavenumber in the ring frame

$$k_r = \sqrt{\frac{\omega}{k_r\ C_\ell}}$$

and x is measured from the junction. The angular velocity at the junction due to the incident wave is:

$$\dot{\theta}_o = \frac{\partial^2 w}{\partial x \partial t} = \omega k_r e^{-i\omega t} \qquad (17)$$

The angular velocity at the junction due to the reflected wave is:

$$\dot{\theta}_r = - M_n\ Y_r \qquad (18)$$

where M_n is the twisting moment at the junction and Y_r is the moment admittance of an infinite beam given by:[4]

$$Y_r = \frac{\omega(1+i)}{4\rho_\ell C_\ell^2 \kappa_r^2 k_r} \tag{19}$$

where ρ_ℓ is the mass per unit length. Similarly, the angular velocity at the spacecraft foot due to the wave transmitted into the spacecraft panels is:

$$\dot{\theta}_s = M_n Y_s \tag{20}$$

where Y_s is the normal moment admittance at the edge of a semi-infinite plate given by:[5]

$$Y_s = \frac{k_s^2}{\sqrt{12}\rho C_\ell \kappa_s^2} \left[0.189 + i\ 0.275 \ln\left(\frac{k_s a}{2.5}\right)\right] \tag{21}$$

where ρ is the plate density and a is one-half the width of the foot. (Eq. 21 is a good approximation for $k_s a < 1$.)

Continuity at the ring-frame, spacecraft-panel junction implies that:

$$\dot{\theta}_o + \dot{\theta}_r = \dot{\theta}_s \tag{22}$$

Combining Eqs. 17, 18, 20, and 22 yields the moment at the junction:

$$M_n = \frac{\omega k_r}{Y_r+Y_s} e^{-i\omega t} \tag{23}$$

and the angular velocity at the junction:

$$\dot{\theta}_s = \frac{\omega k_r Y_s}{Y_r+Y_s} e^{-i\omega t} \tag{24}$$

The time average power flow into the spacecraft panels from one adapter foot is given by:

$$\langle P_{rs} \rangle = \langle R_e(M_n) R_e(\dot{\theta}_s) \rangle$$

$$\langle P_{rs} \rangle = \frac{\omega^2 k_r^2}{2} \frac{R_e(Y_s)}{\left| Y_r+Y_s \right|^2} \tag{25}$$

We now calculate the time-average total energy of the ring frame due to the prescribed incident wave of unit amplitude. The time-average energy associated with the incident wave is:

$$\langle E_r \rangle = \frac{M_r \omega_o^2}{2}$$

Assuming that the magnitude of the reflected wave is approximately equal to the magnitude of the incident wave and neglecting the energy associated with the near field adjacent to the junction, the time average total energy of the ring frame is:

$$\langle E_r \rangle = M_r \omega_o^2 \tag{26}$$

Inserting Eqs. 25 and 26 into Eq. 16 and noting that the total power transferred into the spacecraft panels from the eight feet is eight times the power flow given by Eq. 25, we have:

$$\eta_{rs}^{tor} = \frac{4 k_r^2}{\omega_o M_r} \frac{R_e(Y_s)}{\left| Y_r + Y_s \right|^2} \tag{27}$$

The ring-frame to spacecraft-panel coupling loss factor for torsional motion is calculated from Eq. 27 using the spacecraft parameter values given in Table I and is plotted in Fig. 3.

The octagonal shape of the spacecraft-panel assembly makes it difficult to determine the ring-frame to spacecraft-panel coupling loss factor for radial motion. However, we can calculate an upper bound on this coupling loss factor by ignoring the octagonal shape and calculating the power transmitted by the radial motion for the ring-frame flat-plate system shown in Fig. 2. Proceeding as we did to calculate the torsional coupling loss factor, we find:

$$\eta_{rs}^{rad} = \frac{4}{\omega_o M_r} \frac{R_e(Y_s')}{\left| Y_r' + Y_s' \right|^2} \tag{28}$$

where Y_r' is the force admittance of an infinite beam:[4]

$$Y_r' = \frac{\omega (1+i)}{4\rho \ell C_\ell^2 \kappa_r^2 k_r^3} \tag{29}$$

and Y_s' is the force admittance at the edge of a semi-infinite plate:[5]

$$Y_s' = \frac{1}{\sqrt{12}\rho C_\ell \kappa_s^2} [0.433 + 0.0065i] \tag{30}$$

The ring-frame to spacecraft-panel coupling loss factor for radial motion is calculated from Eq. 28 using the spacecraft parameter values given in Table I and is plotted in Fig. 3.

B. Fixture to Adapter-Stiffener Coupling Loss Factor

To calculate the fixture to adapter-stiffener coupling loss factor, we assume that the fixture moves along a horizontal axis with velocity $v = e^{-i\omega t}$ and consider the adapter stiffeners to be semi-infinite. The force acting between the fixture and an adapter stiffener is given by:

$$F = Z_a' v \tag{31}$$

where Z_a' is the force impedance at the end of a semi-infinite beam:[4]

$$Z_a' = \frac{\rho_\ell C_\ell^2 \kappa_a^2 k_a^3 (1-i)}{2\omega} \tag{32}$$

The time average power transferred into the adapter stiffeners is:

$$\langle P_{fa} \rangle = \langle R_e (F) R_e (v) \rangle$$

$$= 1/2 \, R_e(Z_a') \tag{33}$$

and the time average total energy of the fixture is:

$$\langle E_f \rangle = M_f/2 \tag{34}$$

Substituting Eqs. 33 and 34 into Eq. 16 yields the desired coupling loss factor:

$$\eta_{fa} = \frac{R_e(Z_a')}{\omega_o M_f} \tag{35}$$

The adapter-stiffener to fixture coupling loss factor is calculated from Eqs. 15 and 35 using the spacecraft parameter values given in Table I and is plotted in Fig. 3. We assume the fixture has only one vibration mode, i.e., translation. Although the adapter-stiffener to fixture coupling loss factor plotted in Fig. 3 depends on the

fixture mass, the fixture mass will cancel out in our response calculations so that the ratio of the adapter-stiffener to fixture acceleration is independent of the fixture mass.

C. Adapter Stiffener to Tank Dome Coupling Loss Factor

The adapter stiffener to tank dome coupling loss factor is calculated by assuming that the adapter stiffeners are cantalevered from a flat plate which represents the tank dome. The beam to plate coupling loss factor for this configuration has been studied previously[6] and the result is:

$$\eta_{at} = \frac{2k_a^2}{\omega_o m_a} \frac{R_e(Y_a)}{\left|Y_t+Y_a\right|^2} \tag{36}$$

where m_a is the mass of a single adapter stiffener, Y_a is the moment admittance at the end of a semi-infinite beam:[4]

$$Y_a = \frac{\omega(1+i)}{\rho_\ell c_\ell^2 \kappa_a^2 k_a} \tag{37}$$

and Y_t is the moment admittance at a stud on an infinite plate:[6]

$$Y_t = \frac{\omega}{32\sqrt{\beta}\rho c_\ell^2 \kappa_t^3} [1+i(4/\pi)\ln k_t r] \tag{38}$$

where r is one-half the stud radius and $k_t r < 1$.

The adapter stiffener to tank dome coupling loss factor is calculated from Eq. 38 using the spacecraft parameter values given in Table I and is plotted in Fig. 3.

V. RESPONSE RATIOS

Figures 4-7 present the theoretical response ratios of the elements in the Mariner spacecraft assembly. In each case, the response has been taken to be the space-average mean square acceleration of the element. The theoretical response ratios are calculated from the energy sharing relations (Eqs. 6-9) derived in Section II using the theoretical coupling loss factors shown in Fig. 3 and assuming a value of the internal loss factors of 10^{-2} in every case. Since the response ratios are approximately inversely proportional to the internal loss factors, the response estimates could be considerably improved if experimental data on the internal loss factors (damping) of the elements were available.

Figure 4 presents the ratio of the spacecraft-panel to the adapter-stiffener acceleration calculated assuming transmission via torsional motion and via radial motion at the spacecraft feet. The measured values of the acceleration ratio are greater than those predicted on the basis of torsional motion alone but less than the values predicted on the basis of radial motion. This behavior is in line with our expectations since the power transmission calculation for radial motion neglects the stiffness associated with the octagonal shape of the spacecraft panel assembly and therefore must be viewed as an upper bound.

Figure 5 presents the theoretical and measured ratios of the adapter-stiffener to the test-fixture acceleration in a horizontal vibration test.

Figure 6 presents the theoretical and measured ratios of the spacecraft-panel to test fixture acceleration obtained by multiplying the ratios presented in Figs. 4 and 5.

Figure 7 presents the theoretical ratio of the adapter-stiffener to tank-dome acceleration. This ratio can be multiplied times the ratios presented in Fig. 4 to obtain the theoretical ratio of the spacecraft-panel to tank-dome acceleration inflight. These theoretical acceleration ratios should be compared with flight data at a later date.

The inflight vibration is commonly measured at the spacecraft feet rather than on the adapter or the spacecraft panels. In order to calculate the radial vibration at the spacecraft feet, we have assumed that the ring frame is loaded by the mass of one spacecraft panel at each foot. Proceeding with a wave transmission calculation analogous to that used to derive Eq. 24 (except that here we deal with force and velocity rather than with moment and angular velocity), we can derive the following expression for the ratio of the radial acceleration at the spacecraft feet to the reverberant acceleration of the ring frame:

$$\frac{\langle A^2_{feet} \rangle}{\langle A^2_r \rangle} = \frac{\left| Y_m' \right|^2}{\left| Y_m' + Y_r' \right|^2} \tag{39}$$

where Y_m' is the admittance associated with the lump mass of one spacecraft panel:

$$Y_m = \frac{i}{\omega_o M_s / 8} \tag{40}$$

and Y_r' is the force admittance of the ring frame given by Eq. 29.

Combining Eq. 39 with Eq. 7 and using the spacecraft assembly parameter values given in Table I, yields the theoretical spacecraft-feet to adapter-stiffener response ratio shown in Fig. 8. Measured values of the spacecraft-feet to adapter-stiffener response ratio are also plotted in Fig. 8.

The theoretical values of the response ratios shown in Fig. 4, 5, 6, and 8 are in qualitative agreement with the measured values. Since the discrepancies between the theoretical and measured values are about the same at low and high frequencies, it does not appear practical at this time to refine the theoretical calculations at low frequencies by including the stiffening effects of curvature and the nonresonanct, stiffness controlled transmission--which we have neglected.

REFERENCES

1. E. E. Ungar, "Fundamentals of Statistical Energy Analysis of Vibrating System", AFFDL Technical Report No. AFFDL-TR-66-52, April 1966.

2. J. E. Manning, R. H. Lyon, and T. D. Scharton, "Transmission of Sound and Vibration in a Shroud-Enclosed Spacecraft", BBN Report No. 1431, 1966.

3. E. E. Ungar and T. D. Scharton, "Analysis of Vibration Distributions in Complex Structures", Shock and Vibration Bulletin, 36, 5, January 1967.

4. M. Heckl, "Compendium of Impedance Formulas", BBN Report No. 774, May 1961.

5. E. Eichler, "Plate-Edge Admittances", J. Acoust. Soc. Am., 36, 344-348, February 1964.

6. R. H. Lyon, E. Eichler, "Random Vibration of Connected Structures", J. Acoust. Soc. Am., 36, 1344-1354, July 1964.

TABLE I

Spacecraft Panels

Total mass of 8 panels	1.14 slugs
Total area of 8 panels	3024 $in.^2$
Thickness of panel	0.125 in.

Ring Frame

Total mass of ring frame	0.25 slugs
Total length of ring frame	173 in.
Cross-sectional area of ring frame	0.476 $in.^2$

Adapter Stiffeners

Total mass of 32 adapter stiffeners	0.12 slugs
Length of one adapter stiffener	
a) Adapter stiffener to fixture calculation	20 in.
b) Adapter stiffener to tank dome calculation	40 in.
Cross-sectional area of adapter stiffener	0.08 $in.^2$

Tank Dome

Thickness of the tank dome	0.25 in.

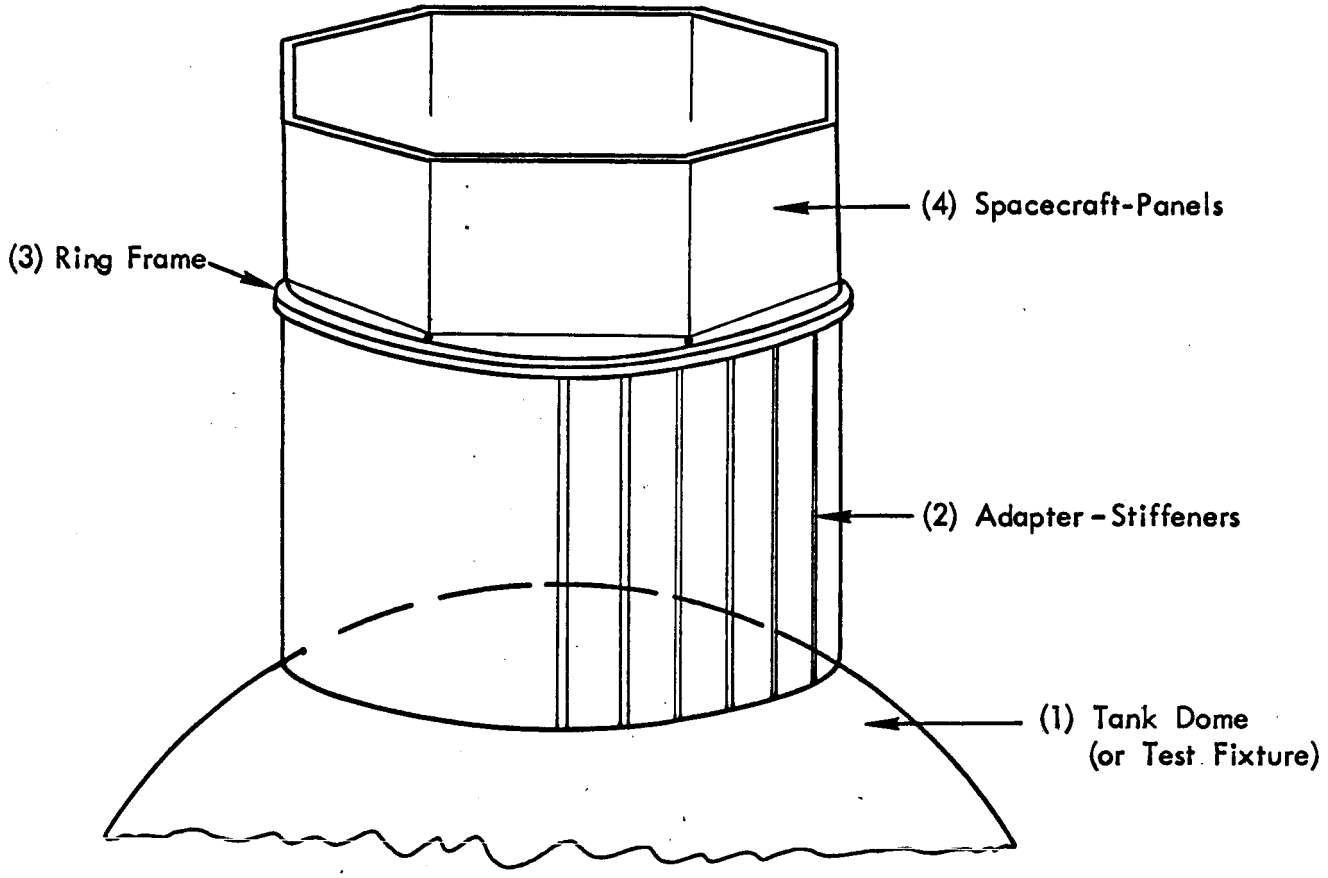

FIGURE 1. VIBRATION TRANSMISSION MODEL OF MARINER '69 SPACECRAFT

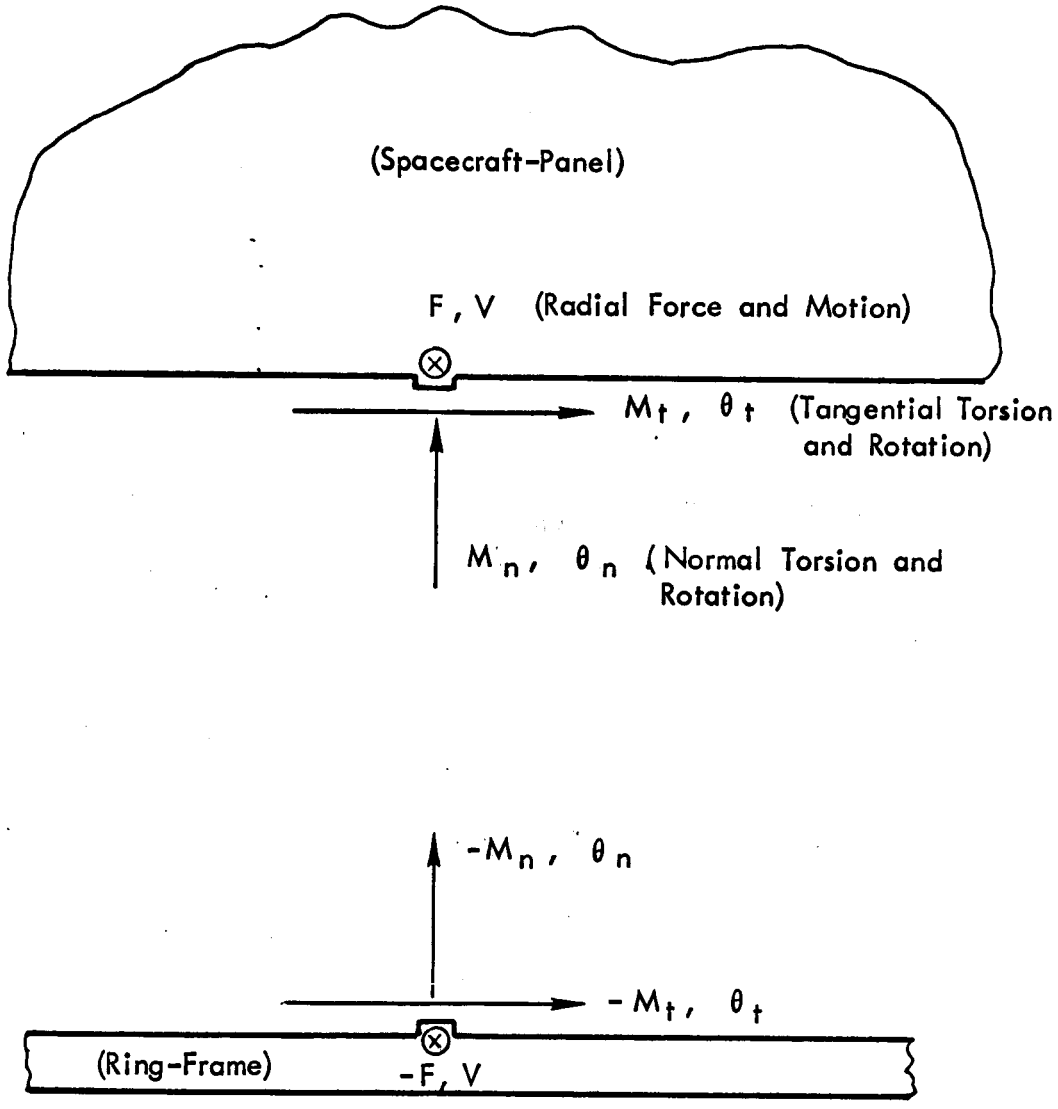

FIGURE 2. CONTINUITY CONDITIONS FOR SPACECRAFT-PANEL AND RING FRAME

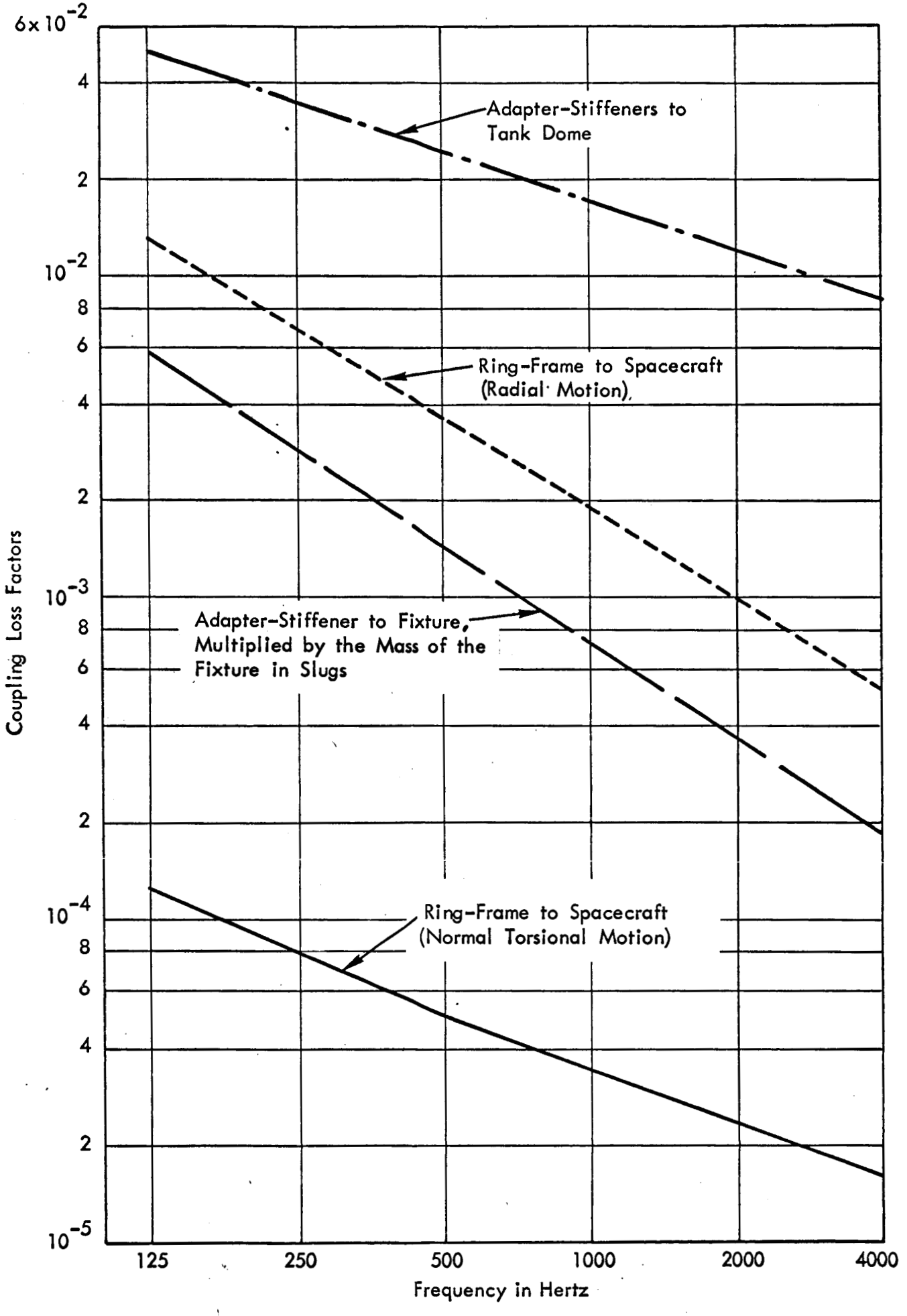

FIGURE 3. COUPLING LOSS FACTORS

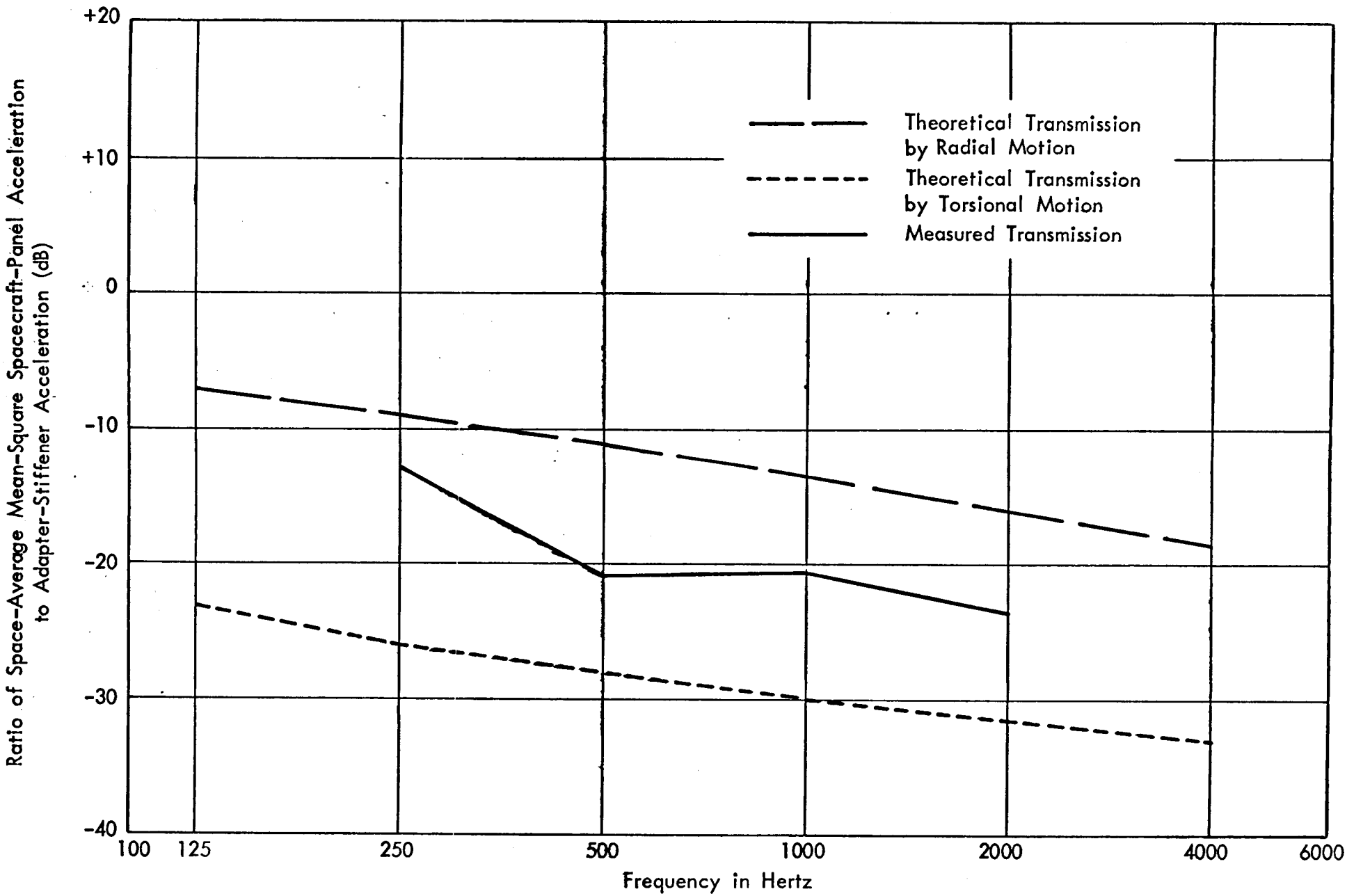

FIGURE 4. RATIO OF SPACECRAFT-PANEL TO ADAPTER-STIFFENER VIBRATION

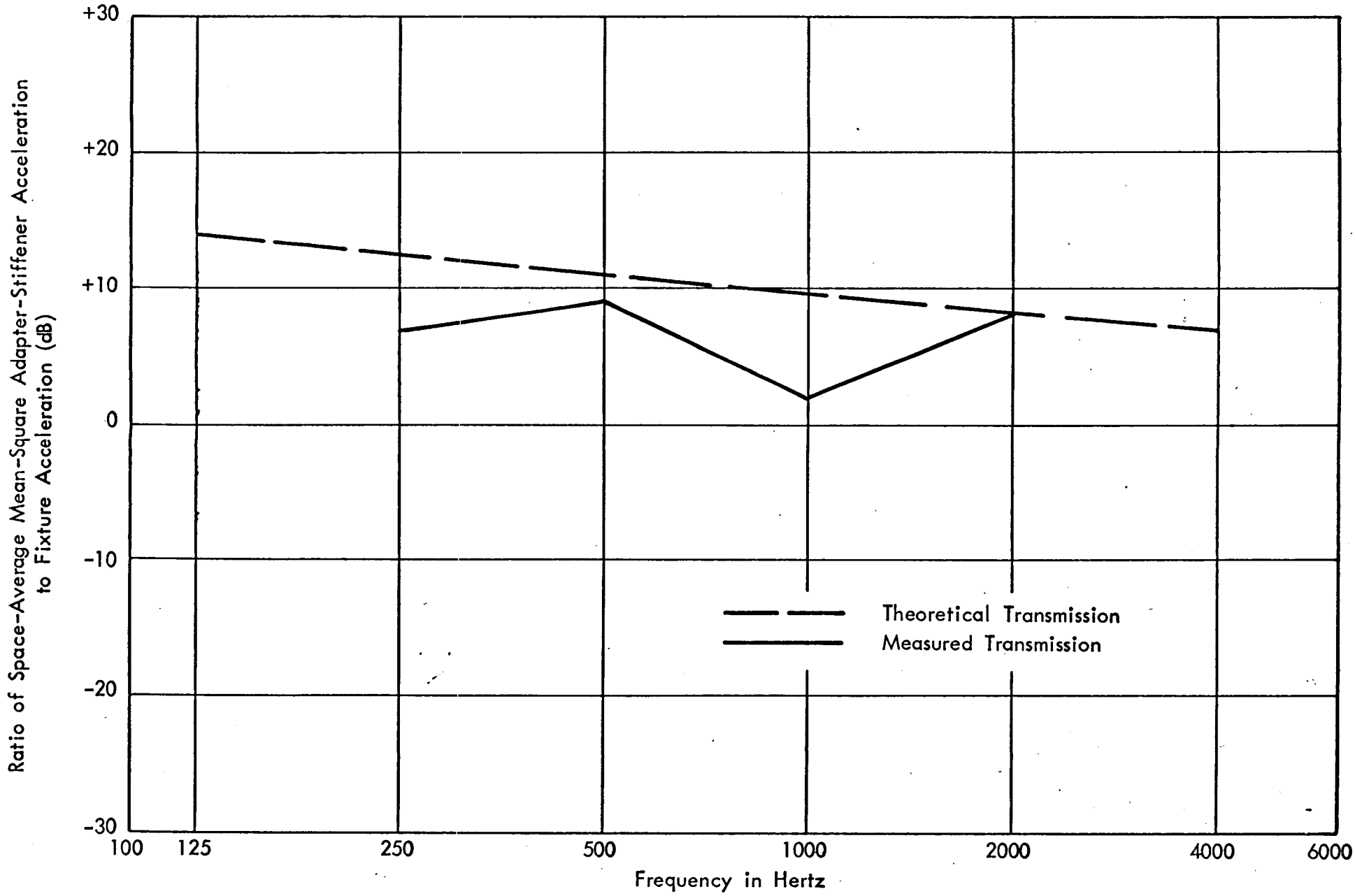

FIGURE 5. RATIO OF ADAPTER-STIFFENER TO FIXTURE VIBRATION

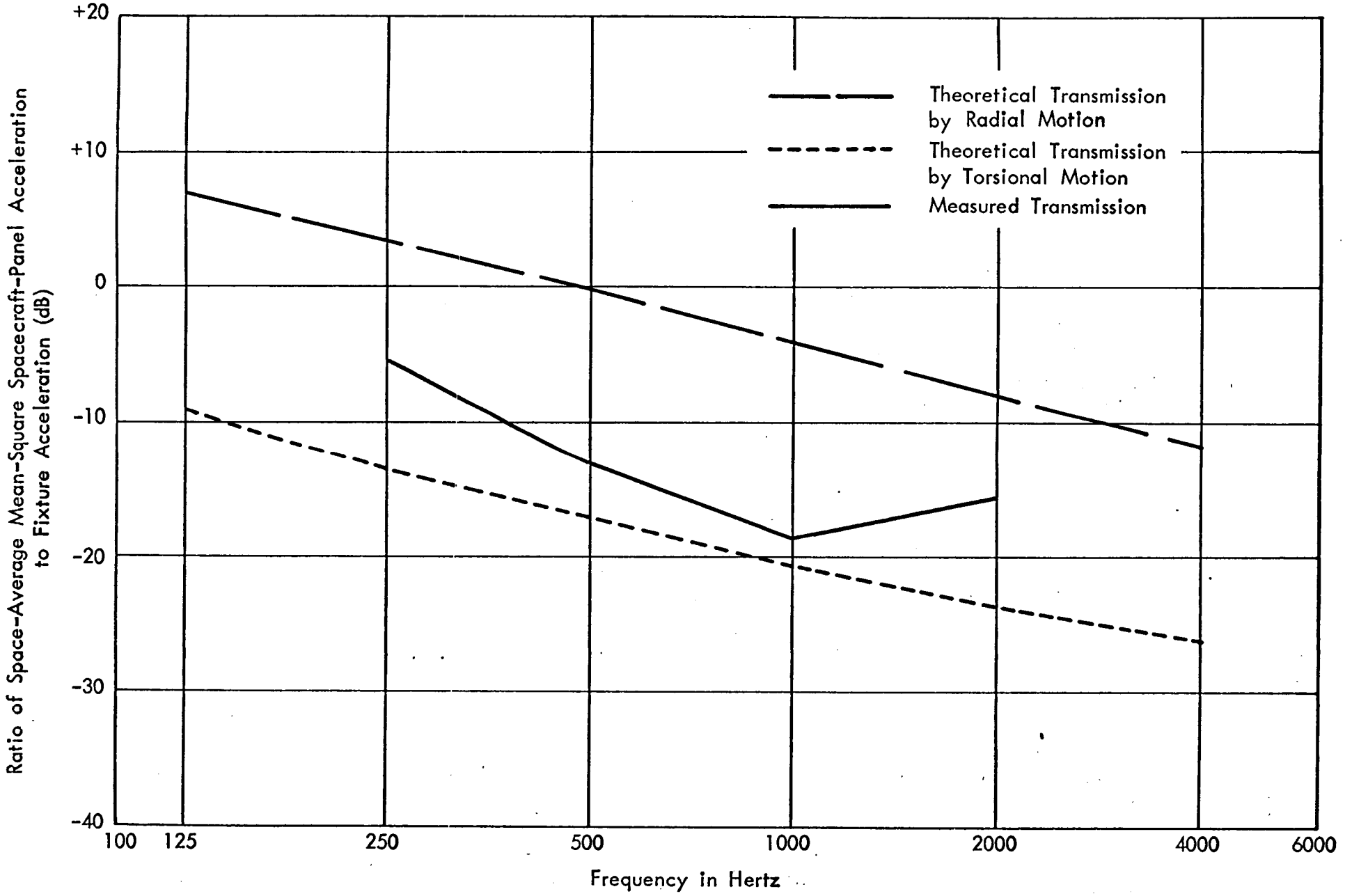

FIGURE 6. RATIO OF SPACECRAFT-PANEL TO FIXTURE VIBRATION

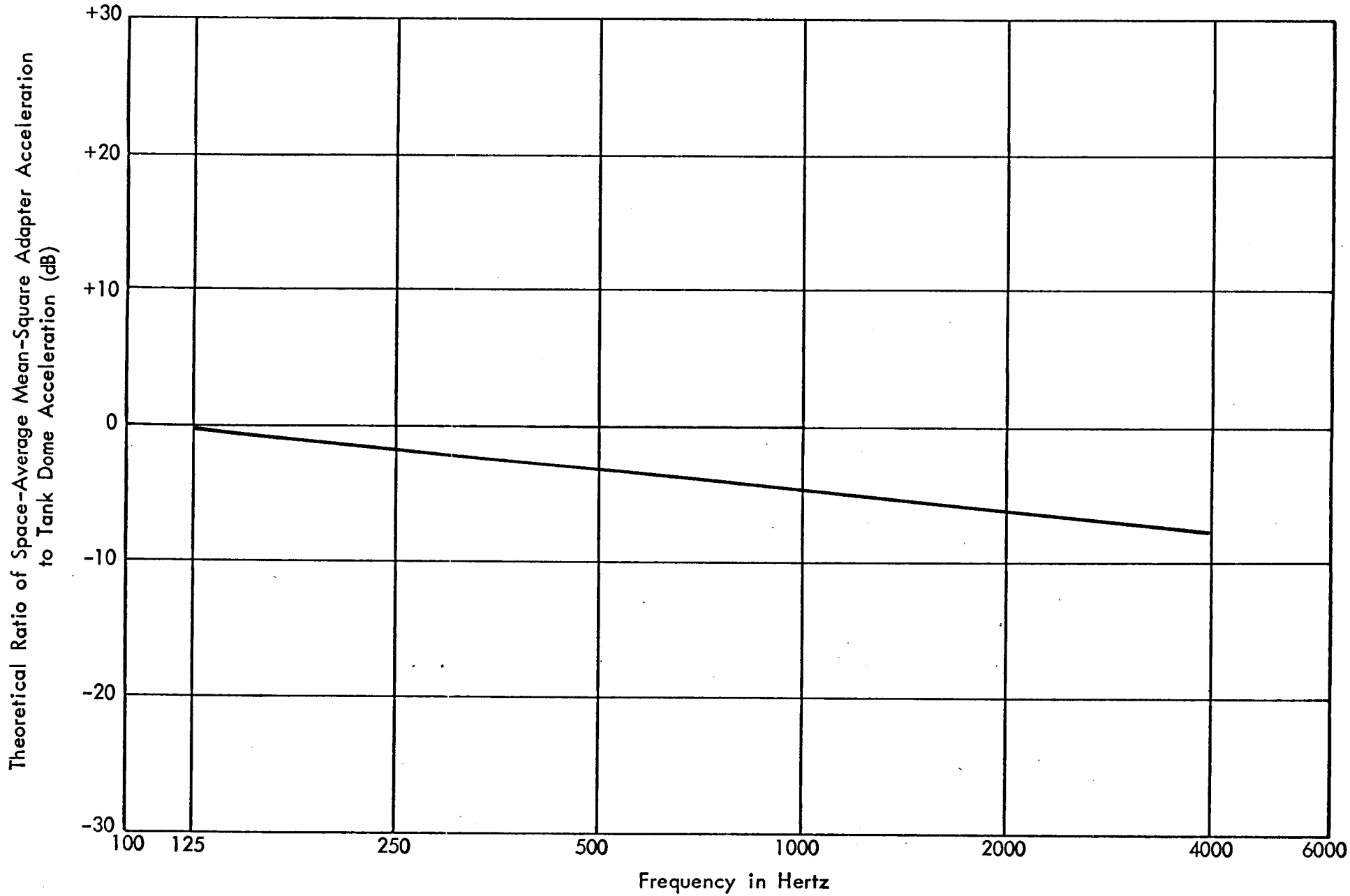

FIGURE 7. THEORETICAL RATIO OF ADAPTER-STIFFENER TO TANK DOME VIBRATION

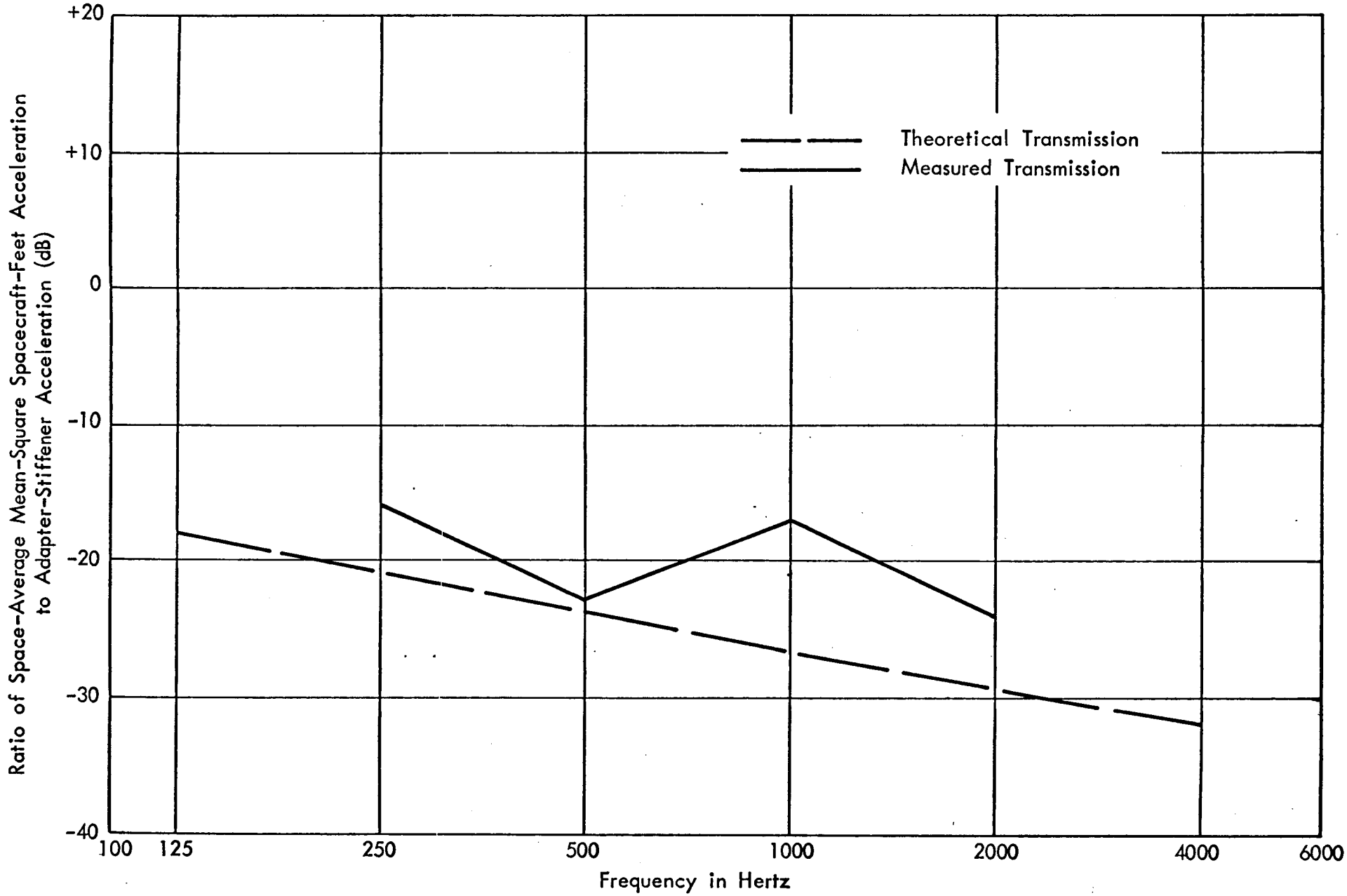

FIGURE 8. RATIO OF SPACECRAFT-FEET TO ADAPTER-STIFFENER VIBRATION

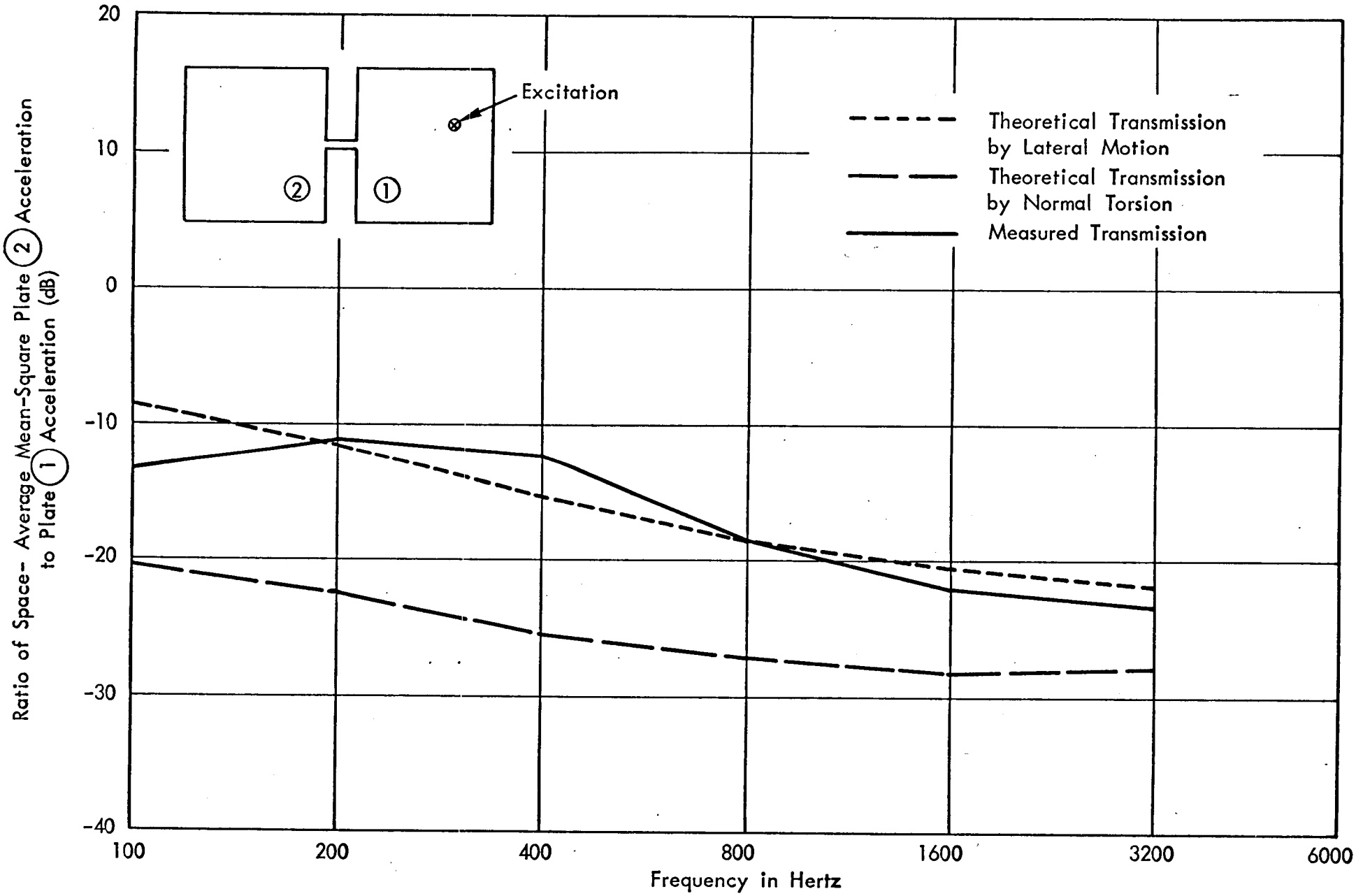

FIGURE 9. VIBRATION TRANSMISSION IN A SIMPLE TWO PANEL STRUCTURE

APPENDIX

An experiment was performed to study the relative importance of torsional and lateral motion in the transmission of power between two plates. In the experimental set-up, two identical aluminum plates were connected with a rod as shown in Fig. 9. The rod was constrained with ball bearings in an attempt to inhibit lateral motion and allow only torsional motion. One of the plates was excited with a small shaker in octave bands of noise and the space-average mean-square acceleration of each plate was measured.

Theoretical and measured values of the ratio of the unexcited plate acceleration to the excited plate acceleration are presented in Fig. 9. The theoretical values of the acceleration ratio for lateral motion were calculated assuming that the bearings were removed and the rod was free to translate as well as rotate. Notice that the theoretical values of the acceleration ratio for lateral motion are approximately 10 dB larger than the theoretical values for torsional motion and agree well with the measured values.

This experiment indicates that even though a structure is constrained so that the lateral motion at a junction between two elements is small, the power transmitted by the small lateral motion may be considerably greater than the power transmitted by torsional motion.